ACSNANO

www.acsnano.org

ARTICLE

Harvesting Broad Frequency Band Blue Energy by a Triboelectric–Electromagnetic Hybrid Nanogenerator

Zhen Wen,[†,‡,§,#] Hengyu Guo,[†,⊥,#] Yunlong Zi,[†,#] Min-Hsin Yeh,[†] Xin Wang,[†] Jianan Deng,[†] Jie Wang,[†] Shengming Li,[†] Chenguo Hu,[⊥] Liping Zhu,[‡] and Zhong Lin Wang*[,†,∥]

[†]School of Materials Science and Engineering, Georgia Institute of Technology, Atlanta, Georgia 30332-0245, United States

[‡]State Key Laboratory of Silicon Materials, School of Materials Science & Engineering, Cyrus Tang Center for Sensor Materials and Applications, Zhejiang University, Hangzhou 310027, China

[§]Institute of Functional Nano and Soft Materials (FUNSOM), Soochow University, Suzhou, Jiangsu 215123, China

[⊥]Department of Applied Physics, Chongqing University, Chongqing 400044, China

[∥]Beijing Institute of Nanoenergy and Nanosystems, Chinese Academy of Sciences, National Center for Nanoscience and Technology (NCNST), Beijing, 100083, China

Supporting Information

ABSTRACT: **Ocean wave associated energy is huge, but it has little use toward world energy. Although such blue energy is capable of meeting all of our energy needs, there is no effective way to harvest it due to its low frequency and irregular amplitude, which may restrict the application of traditional power generators. In this work, we report a hybrid nanogenerator that consists of a spiral-interdigitated-electrode triboelectric nanogenerator (S-TENG) and a wrap-around electromagnetic generator (W-EMG) for harvesting ocean energy. In this design, the S-TENG can be fully isolated from the external environment through packaging and indirectly driven by the noncontact attractive forces between pairs of magnets, and W-EMG can be easily hybridized. Notably, the hybrid nanogenerator could generate electricity under either rotation mode or fluctuation mode to collect energy in ocean tide, current, and wave energy due to the unique structural design. In addition, the characteristics and advantages of outputs indicate that the S-TENG is irreplaceable for harvesting low rotation speeds (<100 rpm) or motion frequencies (<2 Hz) energy, which fits the frequency range for most of the water wave based blue energy, while W-EMG is able to produce larger output at high frequencies (>10 Hz). The complementary output can be maximized and hybridized for harvesting energy in a broad frequency range. Finally, a single hybrid nanogenerator unit was demonstrated to harvest blue energy as a practical power source to drive several LEDs under different simulated water wave conditions. We also proposed a blue energy harvesting system floating on the ocean surface that could simultaneously harvest wind, solar, and wave energy. The proposed hybrid nanogenerator renders an effective and sustainable progress in practical applications of the hybrid nanogenerator toward harvesting water wave energy offered by nature.**

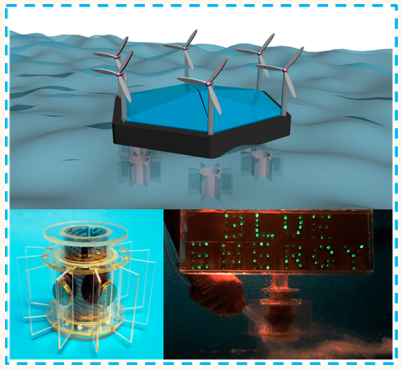

KEYWORDS: *broad frequency band, blue energy, TENG, EMG, hybrid nanogenerator*

Global energy usage has jumped by 45% over the past 20 years, mostly of which is from fossil fuels. To prevent catastrophic warming of the planet, all carbon emissions must be reduced to zero and replaced by 100% clean and renewable energy as a long-term goal.[1−3] Renewables such as solar and wind power offer additional supplements to traditional energies.[4,5] Energy from the ocean, including tidal energy, current energy, wave energy, thermal energy conversion, and osmosis, is abundant.[6,7] However, such blue energy is perhaps the most under-exploited power source owing to engineering difficulties, high cost, and very low efficiency.[8−10] An electromagnetic generator (EMG) is the main approach for harvesting ocean energy, but EMG is rather ineffective in harvesting low frequency mechanical energy, since the output power decays drastically with the decrease of frequency.[11,12] In contrast, the triboelectric nanogenerator (TENG), based on coupling of triboelectrification and electrostatic induction, is effective for low frequency mechanical energy. TENG

Received: May 18, 2016
Accepted: June 6, 2016

DOI: 10.1021/acsnano.6b03293
ACS Nano XXXX, XXX, XXX−XXX

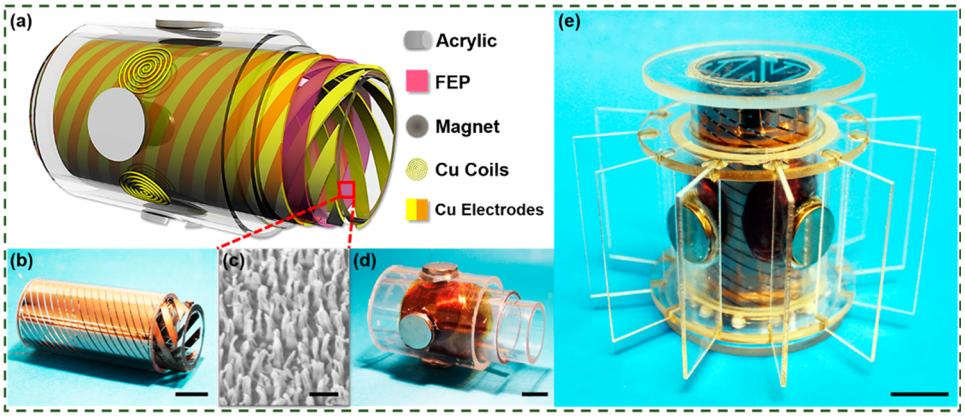

Figure 1. Structure design of the blue energy hybrid nanogenerator. (a) Schematic illustration of the functional components of the hybrid nanogenerator, which mainly consists of a spiral-interdigitated-electrode triboelectric nanogenerator (S-TENG) and a wrap-around electromagnetic generator (W-EMG). Photographs of (b) an as-fabricated S-TENG and (d) an as-fabricated W-EMG (both of the scale bar are 2 cm). (c) SEM image of the FEP polymer nanowires in S-TENG (scale bar, 500 nm). (e) Digital photograph of an as-fabricated hybrid nanogenerator (scale bar, 2 cm).

demonstrates a high energy conversion efficiency, low cost, flexibility, and abundant choice of materials.[13−18] Energy harvesting from broad frequency-band mechanical energy sources such as vibrations, human walking, body motions, and ocean waves has been demonstrated.[19−23] By integrating mature, robust technologies and cutting edge designs with a standardized and modular-based approach, TENG is expected to be a sustainable power source for large-scale application.[24−27] However, a packaging strategy is required that is applicable for the TENGs used in harvesting blue energy without being affected by environmental conditions. Previously, Guo et al. have reported a hybrid nanogenerator consisting of a fully packaged TENG and an EMG with the moving part of TENG indirectly driven by magnets in EMG, which is an ideal model for harvesting blue energy.[28] However, to effectively harvest multidirectional, broad-frequency-range, and varieties of energies in the ocean, further studies on advanced structural designs and characterizations are still required.

Herein, we present a strategy that hybridizes a spiral-interdigital-electrode triboelectric nanogenerator (S-TENG) and a wrap-around electromagnetic generator (W-EMG) for harvesting ocean energy. The hybrid nanogenerator could work under either rotation mode or fluctuation mode to collect the tidal energy, ocean current energy, and wave energy due to the unique structure design. In addition, the characteristics and advantages of outputs from both S-TENG and W-EMG were systematically studied and compared to each other. The results illustrate that S-TENG has more advantages for collecting ocean energy of low frequency than W-EMG, for the purpose of not only directly powering electronic units but also charging energy storage devices, enabling the hybrid nanogenerator to generate electricity in a broad range of working frequencies. An energy-harvesting panel floating on the ocean that could harvest wind, solar, and blue energy was also proposed. This work opens an effective and sustainable approach in the practical applications of the hybrid nanogenerator toward harvesting blue energy in a broad frequency range.

RESULTS AND DISCUSSION

Structure Design. The basic structure of a hybrid nanogenerator consists of two main parts, an S-TENG and a W-EMG, which were fabricated from three coaxially placed cylindrical tubes, as schematically illustrated in Figure 1a. Photographs of the detailed functional components of the hybrid nanogenerator are displayed in Figure S1. The inner and middle tubes that could move relative to each other composed a freestanding mode S-TENG, as shown in Figure 1b. A foam that has been sliced in stripes with various tilted angles was deposited with copper electrodes and attached to the outer surface of the inner tube (Figure S1a−c). This foam, acting as a durable supporting substrate of S-TENG, enhances the robustness and stability significantly and, even more importantly, creates a higher density triboelectric charge due to its elasticity and quick-recovery super-resilient property. Likewise, a piece of FEP thin film that was deposited with copper stripes with the relevant tilted angles was rolled up and fixed onto the inner surface of the middle tube (Figure S1d,e). Nanowires ∼100 nm in diameter and ∼1 μm in length have been synthesized on the FEP film as one triboelectric layer to enhance the surface charge density, as displayed in Figure 1c. Similarly, as exhibited in Figure 1d, the W-EMG part consists of all the three coaxially placed cylindrical tubes with four pairs of magnets evenly fixed on the inside surface of the inner tube (Figure S1a) and the outside surface of the outer tube (Figure S1g). Four copper synclastic twined coils embedded in the outside surface of the middle tube (Figure S1f). By designing adjacent magnets with opposite magnetic polarizations and the adjacent coils with opposite winding directions, the induced current is enhanced to a factor of 2. After mounting a set of rotor blades to the outer tube (Figure S1h,i) to convert the water flow energy into a rotation, a conceptual hybrid nanogenerator was fabricated. A photograph of an as-fabricated hybrid nanogenerator is shown in Figure 1e. By using two encapsulation lids on both ends of the middle tube, the S-TENG part can be fully isolated from the external environment. Detailed information about fabrication can be found in the Experimental Section.

Working Mechanism. The electricity generation of the hybrid nanogenerator can be divided into two modes, the rotation mode and the fluctuation mode, and the energy generated by each mode consists of two parts, one part from S-TENG and another from W-EMG, as schematically depicted in Figure 2. The S-TENG owns spiral-interdigitated-electrode and a corresponding FEP strips, which enables the S-TENG to have

DOI: 10.1021/acsnano.6b03293
ACS Nano XXXX, XXX, XXX−XXX

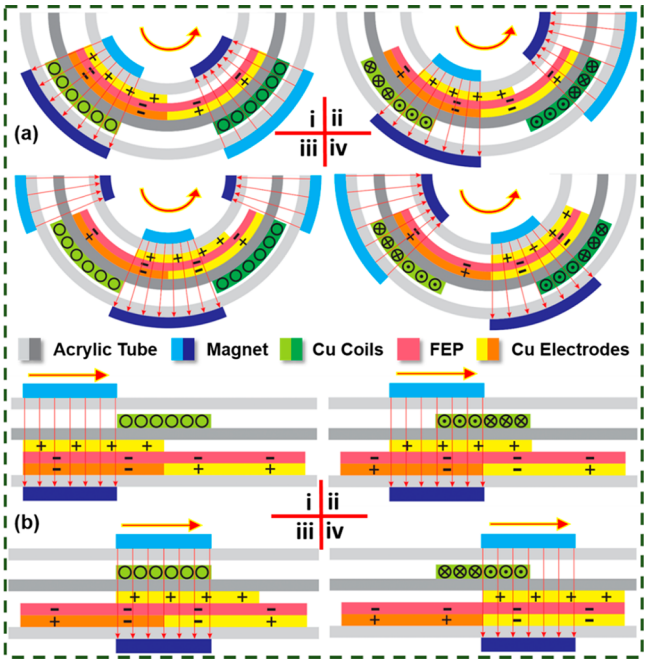

Figure 2. Schematics diagrams of working mechanism of the hybridized S-TENG and W-EMG. The diagrams illustrate schematics of the electricity generation process in a half cycle under (a) rotation mode (cross section) and (b) fluctuation mode (longitudinal section) at four states, indicating the relationship between the direction of current flow of W-EMG, the charge distribution of S-TENG, and the distance of motion.

double dual-function for harvesting both rotational and translational energies (Figure S2).[29] The wrap-around design of W-EMG enables the copper coils to cut the magnetic flux lines under both rotation and fluctuation modes and then generates current output (Figure S3). Since the adjacent magnets have the opposite magnetic polarizations and the adjacent copper coils have the opposite winding directions, in one period the doubled current can be obtained. The attractive forces are formed between pairs of magnets, and the rotator of the S-TENG can be driven by operating the rotator of the W-EMG without direct contact, which is the key strategy to package S-TENG to prevent it from contacting with water.[30,31] Here, we take the rotation mode as an example to discuss electricity generation process in a half cycle, as schematically illustrated in Figure 2a. The operation of the S-TENG is based on coupling of triboelectrification and electrostatic induction.[32−34] Initially, physical contact between triboelectric layers made from copper and FEP creates equal amount of negative and positive charges on the contacted surfaces of layers (i). Then, as triggered by the indirect force of magnets, relative motion between these layers breaks the existing electrostatic balance, which builds a potential difference between electrodes and the negative charges transfer from the original electrode to another copper electrode through the external circuit to rebalance electrostatic status (ii and iii). The charge transfer continues in the whole process until another electrode is fully overlapped and a new equilibrium is established, reaching the final state (iv). Because of the symmetric structure, the rotation beyond the final state until the next initial state induces the reversed potential difference, and hence, the current flows in the opposite direction. Simultaneously, the magnets align and misalign with the copper coils of the W-EMG to create output that is synchronized with that of the S-TENG. When the pairs of magnets are aligned with the coils, no current output due to stable magnetic flux (i). As the magnets in the rotatory part of the W-EMG start to spin, the magnetic flux crossing the coils either decreases or increases, which induces current in the coils to generate a magnetic field that can impede the decrease or increase of the magnetic flux due to Lenz's law (ii). Similarly, the continuous rotation induces the current flow in the reversed direction (iii and iv). The working mechanisms of the S-TENG and W-EMG under fluctuation mode resemble with that under rotation mode. The electricity generation process under fluctuation in a half cycle is schematically illustrated in Figure 2b. Detailed discussion can be found in the Supporting Information.

Electrical Performance. To determine the optimized parameters, we fabricated different types of S-TENG with various spiral degrees (Figure S4) and electrode widths (Figure S5) in which the parameters were defined (Figure S6), and the output performance are discussed in detail in the Supporting Information. Here, we selected a spiral-interdigitated-electrode with the spiral degree of tan θ = 80/101 and the electrode width of 3 mm as the optimized parameters. A rotation motor was employed to simulate the rotatory motion with varied rotation speeds ranging from 10 to 300 rpm, while a liner motor was used to simulate fluctuation motion with operation frequencies ranging from 1 to 5 Hz. The typical power generation performances including open-circuit voltages (V_{OC}), short-circuit currents (I_{SC}), and average power densities under optimized load resistance for both of rotation and fluctuation modes of S-TENG and W-EMG were systematically measured, as shown in Figure 3. As displayed in Figure 3a, the measured V_{OC} of S-TENG under rotation mode stays constant, where the peak values are kept at ∼375 V. Notably, the peak density increased proportionally with the increasing rotation speeds. I_{SC} is proportional to the rotation speeds, raising linearly from ∼1.55 to ∼14.12 μA. For W-EMG, both of V_{OC} and I_{SC} are proportional to the rotation speeds due to Faraday's law. It is observed that V_{OC} raises linearly from ∼0.068 to ∼1.79 V while I_{SC} increases from 0.76 to 11.57 mA, as revealed in Figure 3b. The trend of the output performance of fluctuation motion is similar to that of the rotation mode, as displayed in Figure 3c,d. The electrical output performances under the fluctuation mode with different motion distances were also carried out, as shown in Figure S7. Here, we chose the motion distance of 20 mm as the experimental condition. Under the fluctuation mode, the V_{OC} of S-TENG stays almost constant at ∼360 V and I_{SC} of S-TENG raises linearly from ∼2.10 to ∼8.05 μA, while V_{OC} of W-EMG raises linearly from ∼0.13 to ∼0.51 V and I_{SC} of W-EMG increases from 0.66 to 2.91 mA with the increased operation frequencies. We also experimentally demonstrated correlations between the optimized average power densities and the rotation speeds or operation frequencies for S-TENG and W-EMG fabricated, respectively, as shown in Figure 3e,f. The optimized average power densities of S-TENG are proportional to the triggering frequency (rotation mode: ∼ 1.25 to ∼15.67 μW/cm^2; fluctuation mode: ∼ 0.56 to ∼4.07 μW/cm^2), while that of W-EMG is proportional to the square of the frequency (rotation mode: ∼ 0.11 to ∼27.12 μW/cm^2; fluctuation mode: ∼ 0.03 to ∼6.33 μW/cm^2), as we stated and demonstrated in our previous work.[12] The measured optimized average power subject to the matched external load resistance plots are shown in Figure S8, in which the high output impedance of S-TENG can be lowered by a recently reported power-management

DOI: 10.1021/acsnano.6b03293
ACS Nano XXXX, XXX, XXX−XXX

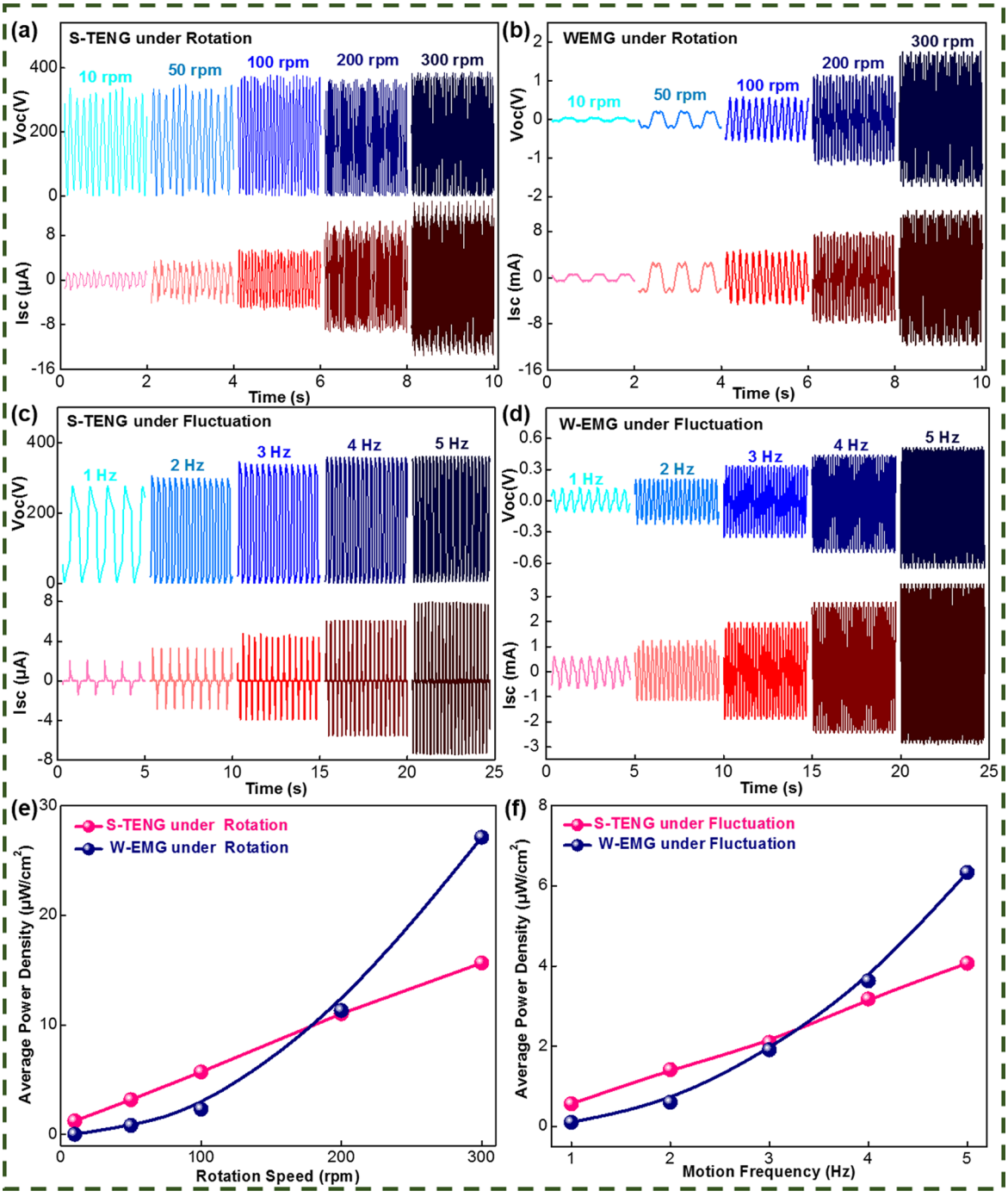

Figure 3. Electrical output performances of S-TENG and W-EMG under two different working modes. The open-circuit voltages (V_{OC}) and the short-circuit current (I_{SC}) under rotation mode at speeds ranging from 10 to 300 rpm of (a) S-TENG and (b) W-EMG. The V_{OC} and I_{SC} under fluctuation mode at frequencies ranging from 1 to 5 Hz with motion distances of 20 mm of (c) S-TENG and (d) W-EMG. The optimized average power densities of S-TENG and W-EMG under (e) rotation and (f) fluctuation modes.

system.[26] The power ratio between S-TENG and W-EMG can be found in Figure S9. The optimized average power for S-TENG and W-EMG are equal for rotation and fluctuation modes at the rotation speed of 175 rpm and operation frequency of 3.3 Hz, respectively, indicating there is always a low-frequency range in which the output performance of S-TENG is better than that of W-EMG, no matter which modes are chosen for comparison.

Distinctive Characteristics. The efficient usage of the energy generated by S-TENG and W-EMG is distinctly different at different rotation speeds and/or operation frequencies. To further evaluate and compare the overall energy output capability for S-TENG and W-EMG, a series of experiments were conducted, as shown in Figure 4. First, we utilized S-TENG and W-EMG to power small electronics, three LEDs under different rotation speeds and operation frequencies, as shown in Figure 4a and b. As measured, the threshold for lighting three LEDs in series or in parallel is ~8.3 or 2.3 V, respectively, while the current required is less than 1 μA (with $I-V$ curve as shown in Figure S10), which can be very easily

DOI: 10.1021/acsnano.6b03293
ACS Nano XXXX, XXX, XXX−XXX

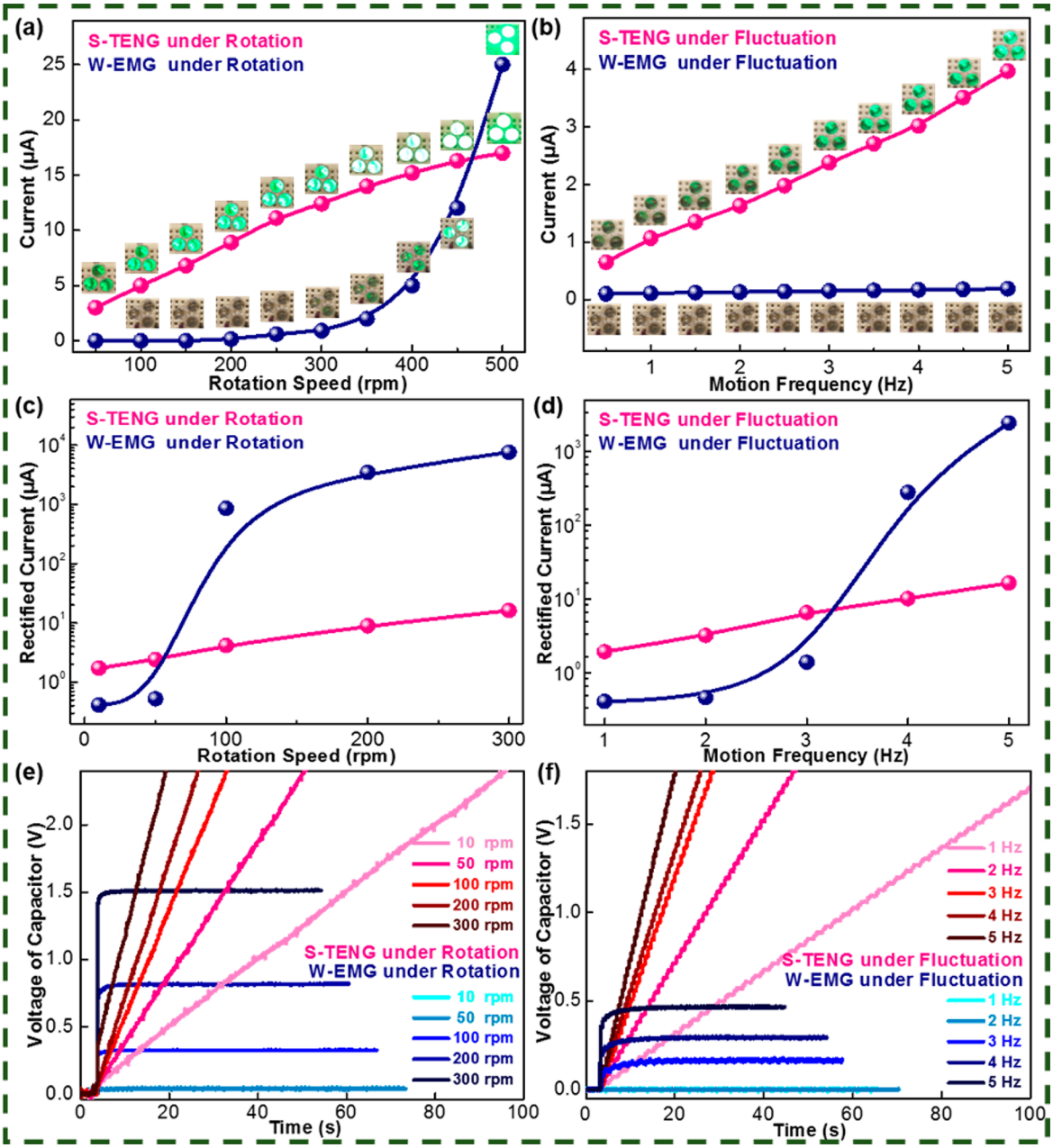

Figure 4. Distinctive ouput performances between S-TENG and W-EMG as a function of operation frequency. The current through three LEDs as driven under (a) rotation mode and (b) fluctuation mode, where three LEDs driven by S-TENG are in series while for W-EMG are in parallel. Insets show the photographs of the lighting LEDs for a visual indication of the generated power. The rectified short-circuit current of S-TENG and W-EMG under (c) rotation mode and (d) fluctuation mode, where a rectifier bridge with the cut-in voltage at 0.2 V was employed. The voltage of capacitors as charged under (e) rotation mode (a 20 μF capacitor used) and (f) fluctuation mode (a 5 μF capacitor used), which indicates the saturation voltages as charged by W-EMG are limited by the low voltage output.

satisfied by S-TENG, even at a quite low rotation speed or operation frequency. However, a certain rotation speed or operation frequency is required to achieve the threshold voltage for W-EMG (~350 rpm for rotation mode; does not work lower than 5 Hz). When the rotation speed reaches 500 rpm, the brightness of LEDs as powered by W-EMG begins to exceed that as powered by S-TENG. Practically, for proper operation, a certain threshold voltage is mandatory for current rectification, management, and storage in order to power electronic units. Therefore, the extremely small output voltage of W-EMG under low rotation speed/operation frequency limits its practical applications. We experimentally measured the rectified current of S-TENG and W-EMG by using full-wave bridge rectifiers, as shown in Figure 4c,d. The detailed rectified short-circuit currents are displayed in Figure S11. It takes at least ~0.2 V in voltage drop to trigger a full-wave bridge rectifier. For S-TENG, due to its high output voltage (~100 V level) and low current (~10 μA level), this voltage drop across the rectifier is negligible and the power loss is very small. But for W-EMG as a low-voltage (~1 V level) and high current (~1 mA level) generator, this voltage drop is relatively significant and the power loss is large, especially for the low-frequency range. In an even lower frequency range (<50 rpm under rotation mode or <2 Hz under fluctuation mode), the

DOI: 10.1021/acsnano.6b03293
ACS Nano XXXX, XXX, XXX−XXX

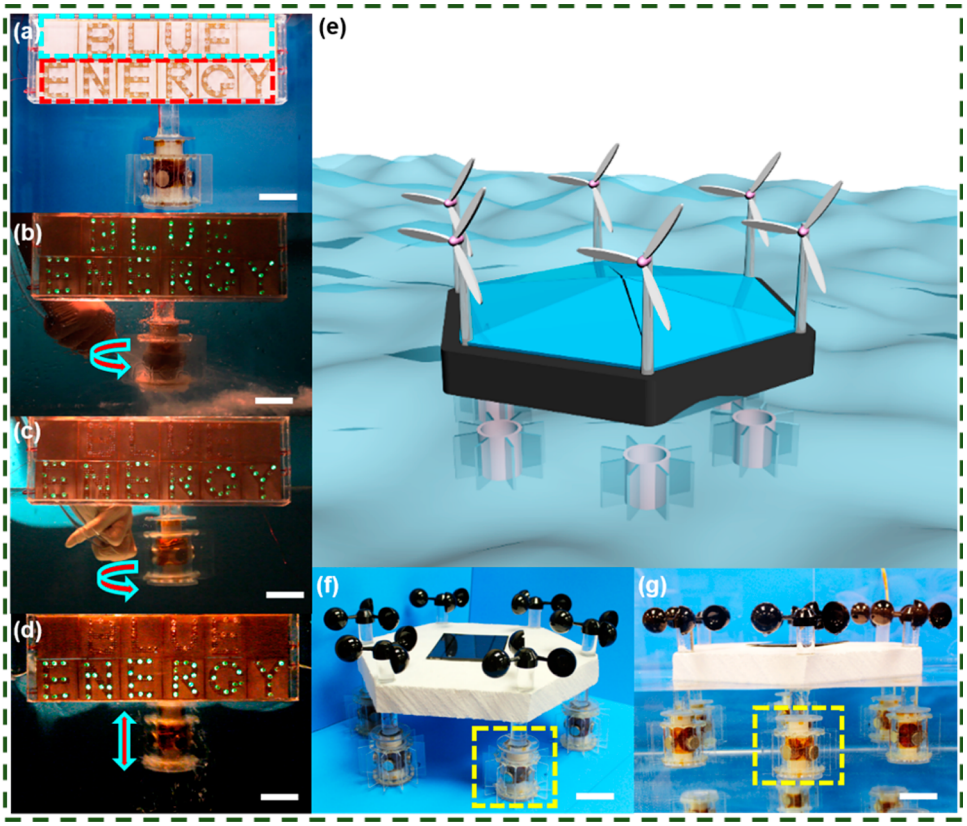

Figure 5. Demonstrations of the hybrid nanogenerator as a practical power source. (a) Photograph of a single unit of hybrid nanogenerator acting as the power source for lighting LEDs. The light blue rectangle frame inside displays 40 green LEDs in parallel composed "BLUE" word that connected to the W-EMG. The red rectangle frame insider displays 58 green LEDs in series composed "ENERGY" word that connected to the S-TENG. A hybrid nanogenerator was used for lighting up the "BLUE" and "ENERGY" LEDs at simulated ocean conditions under (b) rotation mode above the water, (c) rotation mode under the water, and (d) fluctuation mode under the water. (e) Schematic illustration of a proposed comprehensive energy harvesting panel floating on the ocean, which mainly consists of wind-driven generators, solar cell panels, and arrays of hybrid nanogenerators. (f) Oblique-angle-view and (g) lateral-view photograph of the configuration of the hybrid nanogenerator model in ocean-simulated conditions (both the scale bar are 10 cm). The yellow rectangle frame inset is a single unit of the hybrid nanogenerator.

rectified current output become too small to be measured, which shows the ineffectiveness of W-EMG for harvesting low-frequency energy. Only at a large rotation speed (≥200 rpm) or frequency (≥4 Hz), does W-EMG begis to output larger current than that of S-TENG. The low output voltage of the W-EMG at low frequency largely reduces the effective usage of its generated power, which can also be reflected by charging commercial capacitors. The voltages of the capacitors as charged by S-TENG and W-EMG under rotation mode (20 μF for rotation mode) and fluctuation mode (5 μF for fluctuation mode) are shown in parts e and f, respectively, of Figure 4. For S-TENG, it has been demonstrated that the voltage of the capacitors can be charged up to its maximum open-circuit voltage in the level of ∼100 V. Besides, the rate of using the S-TENG to charge a capacitor can be greatly enhanced through the designed charging cycle and the power-management system as reported.[26,35] But for W-EMG, during charging capacitors, the saturation voltage, which is defined as the highest possible voltage achieved, is limited by the low open-circuit output voltage (<50 rpm for rotation mode and <2 Hz for fluctuation mode). The low saturation voltage makes most of the energy from W-EMG unable to be stored and is largely lost. In addition, this limitation makes W-EMG unable to charge an energy storage unit that operates in a higher voltage. Through comparing the characteristics of S-TENG and W-EMG, it is indicated that the outputs of TENG and EMG are complementary for harvesting a broad-frequency-range blue energy, which is achieved by the hybridization process. Transformers can be used for adjusting the output voltages and currents from each part to have a similar output impedance.[28] The circuit diagram of hybridizing S-TENG and W-EMG is shown in Figure S12.

Practical Demonstrations. To explore the capability of the hybrid nanogenerator for large-scale blue energy harvesting as a practical power source, a single unit of hybrid nanogenerator was directly integrated with commercial LED bulbs without using any storage or power regulation units, as shown in Figure 5a. Forty green LED bulbs in parallel making up the "BLUE" word (light blue rectangle frame) are connected to the W-EMG part and 58 green LED bulbs in series are connected to the S-TENG part, which constitute the word "ENERGY" (red rectangle frame). The hybrid nanogenerator was used for lighting the "BLUE" and "ENERGY" LEDs at a simulated ocean environment under different conditions. The circuit diagram of the two lighting system in the practical demonstrations of harvesting blue energy is depicted in Figure S13. For the hybrid nanogenerator above the water under the rotation mode, which is shown in Figure 5b and supporting movie 1, as simulated water flow passed by, the wheel starts to rotate and drive the hybrid nanogenerator, which is capable of

DOI: 10.1021/acsnano.6b03293
ACS Nano XXXX, XXX, XXX−XXX

lighting up the "BLUE" and "ENERGY" LEDs simultaneously. It was noticed that when the rotation speeds were high enough, the output voltage of W-EMG was higher than the threshold voltage of the LEDs, and then the "BLUE" word lit up much brighter than the "ENERGY" word driven by S-TENG due to much higher output current. However, while working underwater, the rotation speeds cannot reach that high due to the huge underwater resistance for the rotation motion; thus, the "BLUE" word cannot be lit up, as shown in Figure 5c and supporting movie 2. Similarly, for the fluctuation mode underwater, only the "ENERGY" word can be lit by S-TENG no matter how low the operation frequency, as shown in Figure 5d and supporting movie 3. The hybrid nanogenerator provides a significantly effective strategy to collect the ocean current, tide, and wave energy from low to high frequency. Furthermore, we propose an energy harvesting panel floating on the ocean, which mainly consists of wind-driven generators, solar cell panels, and arrays of hybrid nanogenerators, as schematically illustrated in Figure 5e. An oblique-angle-view and a lateral-view photograph of the configuration of the energy harvesting panel model in simulated ocean conditions are shown in parts f and g, respectively, of Figure 5. A single unit of the hybrid nanogenerator is marked with a yellow rectangle frame inset.

CONCLUSION

In summary, we demonstrated a hybrid nanogenerator for harvesting water wave based blue energy, mainly including an S-TENG and a W-EMG, which could generate electricity under either rotation mode or fluctuation mode to collect energy from ocean tide, current, and wave due to the unique structure design. In this design, S-TENG can be fully isolated from the external environment through packaging and indirectly driven by the noncontact attractive forces between pairs of magnets, and then W-EMG can be easily hybridized. Due to the irreplaceable and unbeatable characteristics of S-TENG for harvesting low frequencies energy (rotation speeds <100 rpm or motion frequencies <2 Hz), which fits the frequency range for most of the blue energy, and the ability of W-EMG to produce larger output in a high frequency range, the complementary output of S-TENG and W-EMG can be maximized and hybridized for harvesting broad frequency-range blue energy. Finally, a single hybrid nanogenerator unit was demonstrated to harvest water wave energy as a practical power source to drive LEDs directly or charge energy storage devices under different simulated ocean conditions. Based on this hybrid nanogenerator, an energy harvesting panel floating on the ocean is proposed to simultaneously harvest wind, solar and wave energy. The proposed hybrid nanogenerator renders an effective and sustainable progress in the practical applications of the hybrid nanogenerator toward blue energy.

EXPERIMENTAL SECTION

Fabrication of the S-TENG. The S-TENG mainly consists of two coaxially placed cylindrical tubes: One with the length of 2 in. (outer diameter of 1.25 in. and inner diameter of 1 in.) could move relative to another one with the length of 3 in. (outer diameter of 1.5 in. and inner diameter of 1.375 in.) in a rotational or sliding motion. A quick-recovery super-resilient foam (4 × 2 in. area, 1/32 in. thickness) was sliced in stripes by a laser cutter (PLS6.75, Universal Laser Systems) with various tilted angles and various electrode widths. Then, copper electrodes were deposited onto the foam by pulsed vapor deposition (PVD). Finally, the foam was attached to the outer surface of the inner tube as one tribo-material and separated by laser-cutter-defined fine trenches in between. A fluorinated ethylene propylene (FEP) thin film (4.22 × 3 in. area, 100 μm thickness) was selected as another one triboelectric layer. Polymer nanowires array nanostructures were created by a common method reported previously.[36−38] The surface morphology of the FEP thin film was characterized by field emission scanning electron microscopy (Hitachi SU-8010). The piece of FEP thin film was deposited with copper stripes with the relevant tilted angles and electrode widths and rolled up and fixed into the middle tube. The two lead wires were connected, respectively, to the two sets of electrodes, and then an S-TENG was obtained.

Fabrication of the W-EMG. The W-EMG part consists of all the three coaxially placed cylindrical tubes. Four pairs of NdFeB permanent disk magnets (0.875 in. diameter and 0.128 in. thickness) were arranged and evenly fixed on the inside of inner tube and outside of outer tube (outer diameter of 2 in. and inner diameter of 1.75 in.). Four copper synclastic twined coils with a diameter of 1.6 in. were embedded in the outside of middle tube. The adjacent magnets with opposite magnetic polarization as well as the adjacent coils have opposite winding direction. After all the coils were connected, the W-EMG was fabricated.

Assembling of the Blue Energy Hybrid Nanogenerator. Two acrylic rings (outer diameter of 2.8 in. and inner diameter of 1.55 in.) with 12 blades were employed to install a rotor to the outer tube for forming a rotor wheel that could convert the seawater flow into a rotation, and a conceptual hybrid nanogenerator was obtained. Homemade lubricating bearings consist of several PTEF balls (3 mm in diameter) were used here to reduce the mechanical resistance between each part. By using two encapsulation lids on both ends of the middle tube, the hybrid nanogenerator can be fully isolated from the external environment.

Fabrication of the Hybrid Blue Energy Harvesting System. A hexagonal kickboard was used as a template to support the whole simulated blue energy harvesting system. An encapsulated solar panel (130 × 150 mm^2, ALLPOWERS) was installed on the top of the kickboard to collect the solar energy. Six large replacement wind cups (Davis Instruments, AO-30003-58) were evenly fixed at the vertex of the hexagonal kickboard to harvest the wind energy on the ocean. Finally, six hybrid nanogenerators were connected to the kickboard underwater to collect the ocean current, tide, and wave energy of ocean.

Electrical Measurement. The output voltage signal of the hybrid nanogenerator was acquired via a voltage preamplifier (Keithley 6514 System Electrometer) and the output current signal by a low-noise current preamplifier (Stanford Research System SR570). The software platform is constructed based on LabVIEW, which is capable of realizing real-time data acquisition control and analysis.

ASSOCIATED CONTENT

Supporting Information

The Supporting Information is available free of charge on the ACS Publications website at DOI: 10.1021/acsnano.6b03293.

Figures S1−S13 and notes describing the working mechanism of the hybrid nanogenerator, the electrical output performances of S-TENG with different spiral degrees, and the electrical output performance of S-TENG with different electrode widths (PDF)

Movie S1: hybrid nanogenerator working above the water with the rotation mode (AVI)

Movie S2: hybrid nanogenerator working under the water with the rotation mode (AVI)

Movie S3: hybrid nanogenerator working under the water with fluctuation mode (AVI)

AUTHOR INFORMATION

Corresponding Author

*E-mail: zhong.wang@mse.gatech.edu.

DOI: 10.1021/acsnano.6b03293
ACS Nano XXXX, XXX, XXX−XXX

Author Contributions

[#]Z.W., H.G., and Y.Z. contributed equally to this work.

Notes

The authors declare no competing financial interest.

ACKNOWLEDGMENTS

This research was supported by the Hightower Chair Foundation and the "Thousands Talents" Program for Pioneer Researcher and His Innovation Team, China. Z.W. expresses his sincere gratitude to the China Scholarship Council (CSC) for the scholarship to support the study at Georgia Institute of Technology.

REFERENCES

(1) Jacobson, M. Z.; Delucchi, M. A.; Bazouin, G.; Bauer, Z. A. F.; Heavey, C. C.; Fisher, E.; Morris, S. B.; Piekutowski, D. J. Y.; Vencill, T. A.; Yeskoo, T. W. 100% Clean and Renewable Wind, Water, and Sunlight (WWS) All-Sector Energy Roadmaps for the 50 United States. *Energy Environ. Sci.* **2015**, *8*, 2093−2117.

(2) Gielen, D.; Boshell, F.; Saygin, D. Climate and Energy Challenges for Materials Science. *Nat. Mater.* **2016**, *15*, 117−120.

(3) Mitchell, C. Momentum Is Increasing towards a Flexible Electricity System Based on Renewables. *Nat. Energy* **2016**, *1*, 15030.

(4) Chu, S.; Majumdar, A. Opportunities and Challenges for a Sustainable Energy Future. *Nature* **2012**, *488*, 294−303.

(5) Armstrong, R. C.; Wolfram, C.; de Jong, K. P.; Gross, R.; Lewis, N. S.; Boardman, B.; Ragauskas, A. J.; Ehrhardt-Martinez, K.; Crabtree, G.; Ramana, M. V. The Frontiers of Energy. *Nat. Energy* **2016**, *1*, 15020.

(6) Tollefson, J. Power from the Oceans: Blue Energy. *Nature* **2014**, *508*, 302−304.

(7) Schiermeier, Q.; Tollefson, J.; Scully, T.; Witze, A.; Morton, O. Energy Alternatives: Electricity without Carbon. *Nature* **2008**, *454*, 816−823.

(8) Callaway, E. Energy: To Catch a Wave. *Nature* **2007**, *450*, 156−159.

(9) Tollefson, J. How Green is My Future? *Nature* **2011**, *473*, 134−135.

(10) Wang, Z. L. Triboelectric Nanogenerators as New Energy Technology and Self-Powered Sensors - Principles, Problems and Perspectives. *ACS Nano* **2013**, *7*, 9533−9557.

(11) Zhang, C.; Tang, W.; Han, C.; Fan, F.; Wang, Z. L. Theoretical Comparison, Equivalent Transformation, and Conjunction Operations of Electromagnetic Induction Generator and Triboelectric Nanogenerator for Harvesting Mechanical Energy. *Adv. Mater.* **2014**, *26*, 3580−3591.

(12) Zi, Y.; Guo, H.; Wen, Z.; Yeh, M.-H.; Hu, C.; Wang, Z. L. Harvesting Low-Frequency (<5 Hz) Irregular Mechanical Energy: A Possible Killer Application of Triboelectric Nanogenerator. *ACS Nano* **2016**, *10*, 4797−4805.

(13) Wang, Z. L.; Chen, J.; Lin, L. Progress in Triboelectric Nanogenerators as a New Energy Technology and Self-Powered Sensors. *Energy Environ. Sci.* **2015**, *8*, 2250−2282.

(14) Zi, Y.; Niu, S.; Wang, J.; Wen, Z.; Tang, W.; Wang, Z. L. Standards and Figure-of-Merits for Quantifying the Performance of Triboelectric Nanogenerators. *Nat. Commun.* **2015**, *6*, 8376.

(15) Zhu, G.; Chen, J.; Zhang, T.; Jing, Q.; Wang, Z. L. Radial-Arrayed Rotary Electrification for High Performance Triboelectric Generator. *Nat. Commun.* **2014**, *5*, 3426.

(16) Li, Z.; Chen, J.; Zhou, J.; Zheng, L.; Pradel, K. C.; Fan, X.; Guo, H.; Wen, Z.; Yeh, M.-H.; Yu, C.; Wang, Z. L. High-Efficiency Ramie Fiber Degumming and Self-Powered Degumming Wastewater Treatment using Triboelectric Nanogenerator. *Nano Energy* **2016**, *22*, 548−557.

(17) Chen, J.; Yang, J.; Guo, H.; Li, Z.; Zheng, L.; Su, Y.; Wen, Z.; Fan, X.; Wang, Z. L. Automatic Mode Transition Enabled Robust Triboelectric Nanogenerators. *ACS Nano* **2015**, *9*, 12334−12343.

(18) Wu, C.; Wang, X.; Lin, L.; Guo, H.; Wang, Z. L. Paper-Based Triboelectric Nanogenerators Made of Stretchable Interlocking Kirigami Patterns. *ACS Nano* **2016**, *10*, 4652−4659.

(19) Chen, J.; Yang, J.; Li, Z.; Fan, X.; Zi, Y.; Jing, Q.; Guo, H.; Wen, Z.; Pradel, K. C.; Niu, S.; Wang, Z. L. Networks of Triboelectric Nanogenerators for Harvesting Water Wave Energy: A Potential Approach toward Blue Energy. *ACS Nano* **2015**, *9*, 3324−3331.

(20) Wang, J.; Wen, Z.; Zi, Y.; Zhou, P.; Lin, J.; Guo, H.; Xu, Y.; Wang, Z. L. All-Plastic-Materials Based Self-Charging Power System Composed of Triboelectric Nanogenerators and Supercapacitors. *Adv. Funct. Mater.* **2016**, *26*, 1070−1076.

(21) Wen, Z.; Chen, J.; Yeh, M.-H.; Guo, H.; Li, Z.; Fan, X.; Zhang, T.; Zhu, L.; Wang, Z. L. Blow-Driven Triboelectric Nanogenerator as an Active Alcohol Breath Analyzer. *Nano Energy* **2015**, *16*, 38−46.

(22) Kim, H.-J.; Kim, J.-H.; Jun, K.-W.; Kim, J.-H.; Seung, W.-C.; Kwon, O. H.; Park, J.-Y.; Kim, S.-W.; Oh, I.-K. Silk Nanofiber-Networked Bio-Triboelectric Generator: Silk Bio-TEG. *Adv. Energy Mater.* **2016**, *6*, 1502329.

(23) Yang, J.; Chen, J.; Yang, Y.; Zhang, H.; Yang, W.; Bai, P.; Su, Y.; Wang, Z. L. Broadband Vibrational Energy Harvesting Based on a Triboelectric Nanogenerator. *Adv. Energy Mater.* **2014**, *4*, 1301322.

(24) Fan, F. R.; Tang, W.; Wang, Z. L. Flexible Nanogenerators for Energy Harvesting and Self-Powered Electronics. *Adv. Mater.* **2016**, *28*, 4283−4305.

(25) Li, S.; Wang, S.; Zi, Y.; Wen, Z.; Lin, L.; Zhang, G.; Wang, Z. L. Largely Improving the Robustness and Lifetime of Triboelectric Nanogenerators through Automatic Transition between Contact and Noncontact Working States. *ACS Nano* **2015**, *9*, 7479−7487.

(26) Niu, S.; Wang, X.; Yi, F.; Zhou, Y. S.; Wang, Z. L. A Universal Self-Charging System Driven by Random Biomechanical Energy for Sustainable Operation of Mobile Electronics. *Nat. Commun.* **2015**, *6*, 8975.

(27) Wang, X.; Niu, S.; Yin, Y.; Yi, F.; You, Z.; Wang, Z. L. Triboelectric Nanogenerator Based on Fully Enclosed Rolling Spherical Structure for Harvesting Low-Frequency Water Wave Energy. *Adv. Energy Mater.* **2015**, *5*, 1501467.

(28) Guo, H.; Wen, Z.; Zi, Y.; Yeh, M.-H.; Wang, J.; Zhu, L.; Hu, C.; Wang, Z. L. A Water-Proof Triboelectric−Electromagnetic Hybrid Generator for Energy Harvesting in Harsh Environments. *Adv. Energy Mater.* **2016**, *6*, 1501593.

(29) Jing, Q.; Zhu, G.; Wu, W.; Bai, P.; Xie, Y.; Han, R. P. S.; Wang, Z. L. Self-Powered Triboelectric Velocity Sensor for Dual-Mode Sensing of Rectified Linear and Rotary Motions. *Nano Energy* **2014**, *10*, 305−312.

(30) Sudhawiyangkul, T.; Isarakorn, D. *12th International Conference on Design and Optimization of a Small-Scale Linear Electromagnetic Energy Harvester, Electrical Engineering/Electronics, Computer, Telecommunications and Information Technology (ECTI-CON)*, 24−27 Jun 2015; IEEE, 2015; pp 1−6.

(31) Beeby, S. P.; Torah, R. N.; Tudor, M. J.; Glynne-Jones, P.; O'Donnell, T.; Saha, C. R.; Roy, S. A Micro Electromagnetic Generator for Vibration Energy Harvesting. *J. Micromech. Microeng.* **2007**, *17*, 1257−1265.

(32) Yeh, M.-H.; Lin, L.; Yang, P.-K.; Wang, Z. L. Motion-Driven Electrochromic Reactions for Self-Powered Smart Window System. *ACS Nano* **2015**, *9*, 4757−4765.

(33) Niu, S.; Wang, Z. L. Theoretical Systems of Triboelectric Nanogenerators. *Nano Energy* **2015**, *14*, 161−192.

(34) Wang, J.; Wen, Z.; Zi, Y.; Lin, L.; Wu, C.; Guo, H.; Xi, Y.; Xu, Y.; Wang, Z. L. Self-Powered Electrochemical Synthesis of Polypyrrole from the Pulsed Output of a Triboelectric Nanogenerator as a Sustainable Energy System. *Adv. Funct. Mater.* **2016**, *26*, 3542−3548.

(35) Zi, Y.; Wang, J.; Wang, S.; Li, S.; Wen, Z.; Guo, H.; Wang, Z. L. Effective Energy Storage from a Triboelectric Nanogenerator. *Nat. Commun.* **2016**, *7*, 10987.

(36) Guo, H.; Chen, J.; Yeh, M.-H.; Fan, X.; Wen, Z.; Li, Z.; Hu, C.; Wang, Z. L. An Ultrarobust High-Performance Triboelectric Nanogenerator Based on Charge Replenishment. *ACS Nano* **2015**, *9*, 5577−5584.

DOI: 10.1021/acsnano.6b03293
ACS Nano XXXX, XXX, XXX−XXX

(37) Yeh, M.-H.; Guo, H.; Lin, L.; Wen, Z.; Li, Z.; Hu, C.; Wang, Z. L. Rolling Friction Enhanced Free-Standing Triboelectric Nanogenerators and Their Applications in Self-Powered Electrochemical Recovery Systems. *Adv. Funct. Mater.* **2016**, *26*, 1054−1062.
(38) Li, Z.; Chen, J.; Guo, H.; Fan, X.; Wen, Z.; Yeh, M.-H.; Yu, C.; Cao, X.; Wang, Z. L. Triboelectrification-Enabled Self-Powered Detection and Removal of Heavy Metal Ions in Wastewater. *Adv. Mater.* **2016**, *28*, 2983−2991.

DOI: 10.1021/acsnano.6b03293
ACS Nano XXXX, XXX, XXX−XXX